01,14

Grain-boundary segregation effect on the strength in Al bicrystals doped with Mg and Ni. Results of MD-modeling

© L.E. Karkina, I.N. Karkin

M.N. Mikheev Institute of Metal Physics, Ural Branch, Russian Academy of Sciences, Yekaterinburg, Russia

E-mail: lidiakarkina@gmail.com

Received January 28, 2026
Revised February 20, 2026
Accepted February 20, 2026

The effect of the ordered grain-boundary segregations in Al−3 at.%Mg and Al−3 at.%Ni alloys on the grain-boundary (GB) fracture was studied using the atomistic modelling method. It was demonstrated that for symmetrical and asymmetric grain boundaries of a special type Σ5 with a tilt axis ⟨001⟩, the GB fracture resistance of Al−Ni alloy increased significantly compared with Al. For Al−Mg, the effect of Mg segregation on GB was weak, ambiguous, and depended on the type of plane within GB width along which the fracture occurred.

Keywords: segregations, grain boundaries, atomistic modelling, grain boundary facture.

DOI: 10.61011/PSS.2026.02.63377.9028

1. Introduction

Grain boundaries (GB) have a significant impact on such properties of materials as strength, ductility, fracture resistance, corrosion resistance, etc. The structure of GB and their effect on the strength characteristics of alloys, formation of segregation, and phase transformations have been intensively studied in recent decades, both experimentally and theoretically, with the involvement of modeling methods of various scale levels [1–3]. Although the problem of segregations at grain boundaries has attracted the attention of researchers for many years, their effect on the structure and properties of grain boundaries remains a matter of argument. The role of segregation along grain boundaries becomes especially important in ultrafine-grained materials, where the proportions of atoms along grain boundaries and in volume are comparable [2,3]. In this case, the formation of segregations at grain boundaries significantly changes the conditions of phase equilibrium [4–6] and thermal stability of the microstructure [7,8]. The alloys Al−Mg and Al−Zn are vivid examples of the significant dependence of segregation on the chemical composition of the doping elements. In particular, for Al−Mg system, it was observed that Mg atoms tend to form heterogeneous agglomerations at the grain boundaries of [4,9], which leads to additional hardening. However, the nature of the observed segregation specifics is still not precisely known.

Computer modeling methods such as density functional theory, molecular dynamics, and others are an important addition to experimental observations of the behavior of segregation at grain boundaries. The results of atomistic modeling of impurity segregation at grain boundaries make it possible to identify important parameters related to the characteristics of grain boundaries (energy, structure, and excess volume), as well as the characteristics of the impurity atom (enthalpy of dissolution, ionic radius). For instance, in [4] it was shown that in Al alloys the segregation at GB of such impurities as Zn, Mg, Cu, may sufficiently raise the stability of the ultra-fine grains in the alloys compared to pure Al. In some theoretical papers [5–8] the decohesis phenomenon at GB in Al decorated with the impurities mentioned above was studied. The main attention was paid to the study of special symmetric GB separating two grains along a plane with low Miller indices. Even in these cases, contradictory results were obtained. Thus, in [6,8] it was shown that Mg segregation leads to a slight increase in grain boundary decohesis, whereas in [5,7] a decrease in the cohesive strength of Al decorated with Mg was obtained. In [9] it is shown that the effect of hardening or loss of strength depends on the concentration of impurity atoms placed in energetically favorable positions near GB: for an isolated impurity, Mg atoms exhibit an embrittlement effect, and in case of rising concentration — strengthening effect.

In [10], it was found that during the segregation of doping elements, the area near the grain boundary may undergo a structural reconstruction. Moreover, as shown in [10,11], even the formation of thin (single-layer) segregations can lead to a significant change in the structure of GB. The nature of GB reconstruction depends on the type of boundary, as well as on the characteristics of the chemical bond between the atoms of the doping element and the matrix. The situation is even more complicated for general-type GB or boundaries that deviate from special symmetrical GB. It has recently been found in [12–14] that the formation of segregation of doping elements can cause nano-faceting of an asymmetric GB. The complex processes of GB restructuring lead to a change in a number of its properties, in particular, the processes of slipping through the GB become more complicated [12].

In atomistic modeling of grain boundary fracture, we used a well-proved rigid-grain-shift (RGS) methodology and RGS + relaxations methodology [15]). In this scheme FP (fracture path) is set either using a plane or a more complex surface allowing for the GB symmetry. This model is applicable in case when the grain-boundary crack growth occurs significantly faster than the rate of impurity diffusion both in the matrix and along the GB. This condition is realized when the deformation occurs in the moderate temperatures region. In the review [16], various scenarios of deformation of nanostructured (NS) materials were considered, mainly related to the processes occurring on GB: grain boundary slippage and nucleation of microcracks in the triple joints of grains caused by the transfer of deformation along the GB from one grain to another. In this case, the opening of cracks along the GB occurs in the plane of the neighboring grain boundary and is mainly determined by the grain boundary deformation of the first grain [17]. When modeling the opening of GB cracks in NS materials, the rigid-grain-shift is, apparently, preferable.

This document outlines the study of the grain-boundary decohesis in Al bicrystals and Al−3 at.%Mg and Al−3 at.%Ni alloys for the dedicated symmetrical and nonsymmetrical grain-boundaries with ⟨001⟩ tilt axis after formation of segregations at GB as realized using MD/MC-modeling. The results allowed to shed light on behavior of Mg and Ni during grain-boundary fracture of aluminum alloys bicrystals containing ordered grain-boundary superstructures.

2. Modelling method

The atomistic modelling of fracture in the bicrystals of Al, Al−3 at.%Mg and Al−3 at.%Ni alloys was carried out for the symmetrical GB of tilt Σ5{012} and Σ5{013} with the disorientation angle $\theta = 36.87^\circ$ (Figure 1, *a, b, e, f, i, k*), corresponding to the minimal elastic energy for Al [18], as well as for the two dedicated asymmetrical grain boundaries Σ5{010}/{340}⟨001⟩ and Σ5{110}/{710}⟨001⟩ (Figure 1, *c, d, g, h, l, m*). The energy of the considered asymmetric GB for Al differs by less than 10 % from the energy of symmetric GB Σ5{210} and Σ5{310} with the same tilt axis ⟨001⟩ [18]. Both asymmetric boundaries are made of the two types of planes: low-index closely-packed planes in the FCC-lattice {110} and {100} from one side of the GB; and highly-indexed planes {710} and {340} —- on the other side.

When modelling Al−Mg alloys we used the potential Lee et al [19]; for Al−Ni alloy — EAM/alloy potential [20]. The potentials correctly describe many physical properties of both pure Al and Al−Mg and Al−Ni alloys. In particular, the potentials give energy values for the formation and interaction of the point defects and their complexes that are close to the results obtained in *ab initio* calculations [21]. Data for the point defects are necessary input parameters for modeling the kinetics of formation of precipitates in the alloys. Numerical analysis was carried out using LAMMPS software package (Sandia National Laboratories) [22].

In all cases, YZ plane coincided with the plane of the boundary, OZ axis was parallel to the tilt axis ⟨100⟩ (see Figure 1). The crystallite contained two grains separated by the studied boundary, located in its center. In all cases, the grain size along OX direction perpendicular to the GB plane was ∼ 20 nm. Periodic boundary conditions were applied in two mutually perpendicular directions OY and OZ in the GB plane. The length of the period along these directions was a multiple of the translation along the specified crystallographic directions. During modeling, the crystallite contained $\sim (4-8) \cdot 10^4$ atoms, depending on the type of grain boundary. Time step was 1.5 fs.

The formation of segregations and structural changes in the GB were modeled using a combined MD/MC approach at a temperature $T = 450$ K. We used the Metropolis scheme [11], which at every MC step additionally included relaxation of MD crystallite with an atom of solute in a new test position, and the probability of an atomic hop was determined taking into account the energy change due to relaxation. Such step-by-step relaxation in MD/MC modeling plays an important role in correctly describing the structural rearrangement of grain boundaries in alloys with a closely packed FCC lattice, including Al−Mg and Al−Ni alloys. In Al matrix, the interaction of impurity atoms with grain boundaries leads to their structural reconstruction during segregation and formation of highly ordered segregation superstructures (in the classification [23]). The occurrence of GB superstructures is controlled by several factors, including the crystallographic parameters of GB, the characteristics of the dissolved or impurity atom, the energy associated with the distribution of the impurity atom near GB sites, and others.

In GB structure (Figure 1) thin green lines designate the structural units [18], that define the local atomic configuration of the boundary. Figure 1, *a*−*d* illustrates the fragments of crystallites, containing symmetric and asymmetric GB for Al. The geometry of asymmetric boundaries can be described in the language of distorted structural units B and C [18], peculiar to the symmetric GB Σ5{210} and Σ5{310}. For GB Σ5{010}/{340}⟨001⟩ the structural units B, C are alternating; each pair with a shift $1/2\langle 001\rangle$ along the tilt axis. For GB Σ5{110}/{710}⟨001⟩ the structural units B, C are alternating in a sequence C, B, B.

The GB configurations for Al shown in Figure 1, *a*−*d* were used as starting configurations during MD/MC modeling in Al−Mg and Al−Ni alloys, which leads to the structural reconstruction of GB in the process of segregation and formation of GB superstructures from impurity atoms. For all types of GB, the alloys exhibit the same regular alternation of structural units as in Al. For Al−Mg the structural unit C changes insufficiently, Mg atoms are located in its center; structural unit $B \rightarrow B_1$ (Figure 1, *e*−*h*). The structural unit B_1 can be considered as a more or less distorted structural unit B with an impurity atom located in its center. In all cases the grain boundaries for

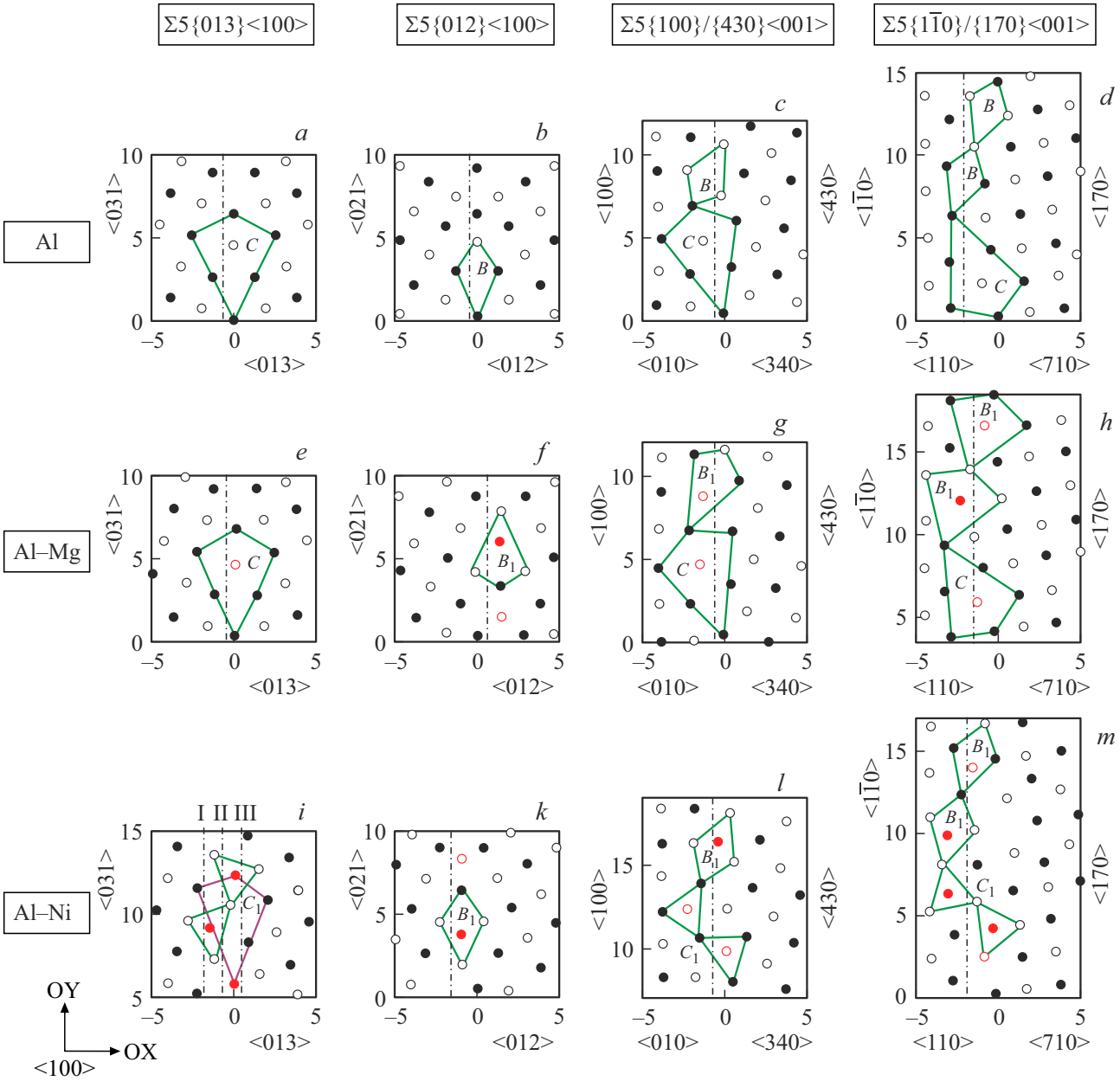

Figure 1. Fragments of crystallites with spetial type symmetrical (a, b, e, f, i, k) and asymmetrical (c, d, g, h, l, m) GB with the tilt axis ⟨001⟩ for Al, Al−3 at.%Mg and Al−3 at.%Ni after 10^6 MD/MC of relaxation steps [10−14]. The light and dark circles correspond to the atoms in the nearest {001} planes. Black color denotes Al atoms, red color — impurity atoms (Mg or Ni). Structural elements are delineated by thin green lines. Dimensions of coordinate axes are given in Å.

Al−Mg after the end of MD/MC-relaxation and boundaries reconstruction a monoatomic (Figure 1, e−g) or close to the monoatomic (Figure 1, h) layer of Mg atoms is formed.

A completely different situation is observed in Al−Ni alloy. Already for the symmetric boundary Σ5{310}⟨001⟩, Ni atoms form a double layer near GB (Figure 1, i); its position shifts and the shape of the structural element $C \rightarrow C_1$ changes. Even a more complex configuration, layered with Ni atoms, is peculiar to the asymmetric GB. As a result, after the MD/MC relaxation is completed, the grain boundaries in Al−Ni acquire a stepped shape consisting of nanofasets (Figure 1, l, m). As discussed in [11–14], the nature of the structural reconstruction of GB and the shape of grain boundaries in alloys are largely determined by the segregation energy of the impurity atom and its most energetically advantageous position near the GB.

3. Modeling results

In the rigid-grain-shift, the separation energy E^i_{sep} when opening a crack at a distance X_i normal to the crack

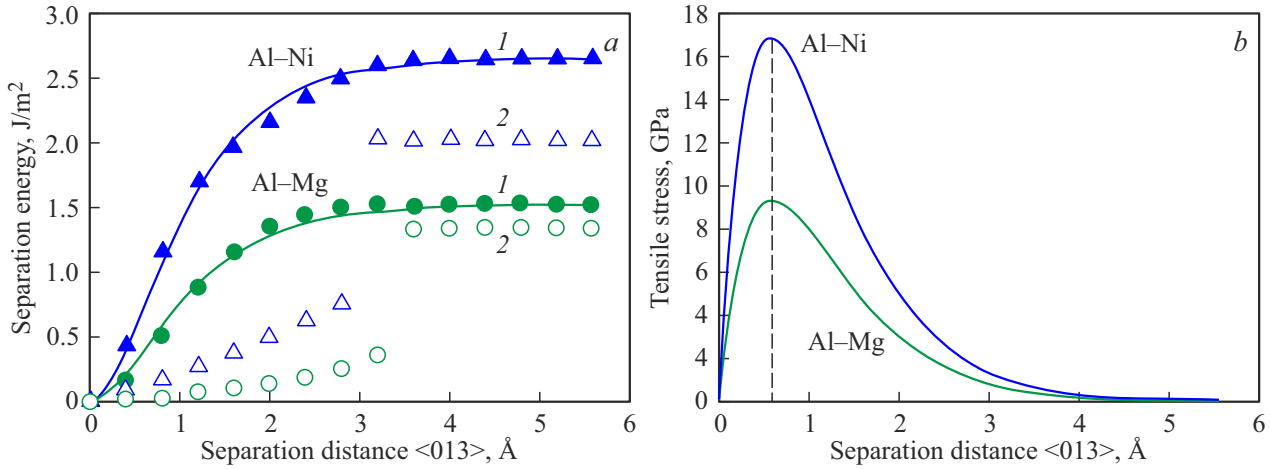

Figure 2. Variation of the separation energy (a) and theoretical tensile stress (b) in opening the crack along GB $\Sigma5\{013\}\langle100\rangle$ in Al−Mg and Al−Ni alloys. *1* — without relaxation, *2* — with relaxation. Blue dots and curves relate to Al−Ni, green — to Al−Mg.

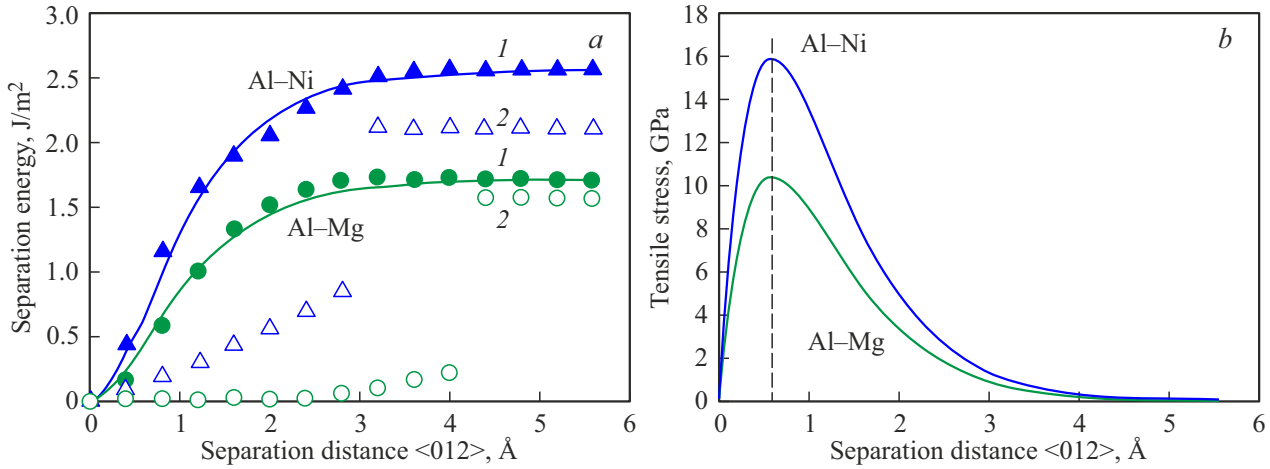

Figure 3. Variation of the separation energy (a) and theoretical tensile stress (b) in opening the crack along GB $\Sigma5\{012\}\langle100\rangle$ in Al−Mg and Al−Ni alloys (section I). *1* — without relaxation, *2* — with relaxation. Blue dots and curves relate to Al−Ni, green — to Al−Mg.

plane was calculated as the difference between the bicrystal energies at a given shear E_i and in the initial configuration E_0, attributed to the grain boundary area:

$$E^i_{\text{sep}} = (E_i - E_0)/S. \quad (1)$$

Fracture energy was found as [6]:

$$E_{\text{frac}} = \lim_{i\to\infty}(E_i - E_0)/S. \quad (2)$$

Approximation of dependence $E^i_{\text{sep}}(X_i)$ for the curve neglecting the relaxation was carried out using expression [6]:

$$E^i_{\text{sep}}(X_i) = E_{\text{frac}} - E_{\text{frac}}(1 + X_i/\lambda)\exp(-X_i/\lambda), \quad (3)$$

where λ — characteristic separation length. The theoretical tensile stress was found using formula $\sigma = \partial E^i_{\text{sep}}/\partial X_i$; the maximum tensile stress in accordance with (3) is then equal to $\sigma_{\max} = E_{\text{frac}}/(e\lambda)$.

3.1. Fracture along symmetric GB $\Sigma5\{013\}\langle100\rangle$ and $\Sigma5\{012\}\langle100\rangle$

In Figure 1, *a, b, e, f, i, k* the vertical dotted line denotes the planes along which the section was cut when opening the cracks for the symmetric GB $\Sigma5$ in Al and in Al−Mg, Al−Ni, alloys containing the grain-boundary segregations superlattices. The impurity atoms form single-layer chains for all variants, except for $\Sigma5\{013\}\langle100\rangle$ boundary for Al−Ni (Figure 1, *i*), where Ni atoms form the two-layer chains. In the latter case, two different cross-sections (I or II) are possible to open cracks near the GB. I and III cross-sections are equivalent.

Figures 2, *a*, 3, *a* illustrates the curves of the separation energy E^i_{sep} variations (formula (1)) inAl−Mg and Al−Ni alloys for the symmetric grain boundaries $\Sigma5\langle100\rangle$. For the curves obtained neglecting the relaxation (curves *1*),

The decohesis energy E_{frac} (J/m^2), σ_{max} (GPa) during the crack opening in Al−Mg and Al−Ni alloys near the symmetric grain boundaries Σ5

GB Σ5{013}⟨100⟩			
Material	E_{frac} Without relaxation With relaxation	E_{frac} *ab initio*	σ_{max}
Al	1.68 1.59	1.64 [21] 1.48	–
Al−Mg	1.52 1.34	1.62 [21] 1.60	9.34
Al−Ni sec II	2.59 1.94	–	16.1
Al−Ni sec I	2.65 2.02	–	16.8
GB Σ5{012}⟨100⟩			
Material	E_{frac} Without relaxation With relaxation	E_{frac} *ab initio*	σ_{max}
Al	1.75 1.73	1.76 [9] 1.57	–
Al−Mg	1.71 1.57	1.73−1.66 [9] 1.56−1.59	10.5
Al−Ni	2.56 2.11	–	16.0

an approximation was performed in accordance with the formula (3), and the theoretical tensile stress was calculated. The curves $\sigma(X_i)$ are shown in Figures 2, *b*, 3, *b*. The table below shows the values of the decohesis energy E_{frac}, maximum tensile stress σ_{max} for Al and its alloys Al−Mg and Al−Ni for the two types of symmetric GB Σ5. The well-known literature data on the energy of decohesis for the same GB, obtained in *ab initio* analysis, are also given.

By comparing the curves for Al−Mg and Al−Ni in Figures 2, *a* and 3, *a* we may see that, in general, the curves for Al−Ni alloy lie higher than for Al−Mg alloy, when both, neglecting and taking into account the relaxation. For both grain boundaries, the change in the decohesis energy E_{frac} during relaxation is significantly higher for Al−Ni alloy compared with Al−Mg alloy; however, at short distances, up to the moment of formation of two free surfaces during separation, the energy change during relaxation is comparable for both alloys. The tensile stress curves, as well as the values of σ_{max} , are also significantly higher for Al−Ni alloy.

The table below provides the numerical values E_{frac}, σ_{max} for Al and its Al−Mg and Al−Ni alloys, obtained in MD calculations using the potentials [19,20]. Also data of *ab initio* analysis of E_{frac} are provided from the literature. In all cases, the upper number is the value of E_{frac} without relaxation, the lower number is the value taking into account relaxation. For GB (013)⟨100⟩ *ab initio* calculations demonstrate weak hardening of $\sim(5-7)\,\%$ upon segregation of Mg atoms at GB (taking relaxation into account) and equally insignificant loss of strength (neglecting the relaxation) compared with GB in Al. MD analysis with the potential [19] also gives an insignificant loss of strength. For the GB (012)⟨100⟩ *ab initio* analysis for Al and Al−Mg are practically equivalent. MD analysis provides an insignificant loss of strength within $\sim(5-10)\,\%$. Thus, it can be assumed that the changes in the decohesis energy in Al−Mg alloy compared with Al for the symmetric GB Σ5 of both types are insignificant. The values E_{frac} are within the range of both the calculated and measurement errors.

Another situation is valid for Al−Ni alloy (potential [20]). For both types of symmetric GB, Ni segregations significantly strengthen GB, increasing the values of E_{frac} by approximately $(20-35)\,\%$. The value σ_{max} grows by $\sim 40\,\%$. Unfortunately, there is currently no data on *ab initio* analysis of decohesis in Al−Ni alloy. Thus, it can be argued that in MD calculations, Ni segregations give a significant strengthening of grain boundaries compared to Al.

3.2. Fracture along asymmetric GB Σ5{010}/{340}⟨001⟩ and Σ5{110}/{710}⟨001⟩

Already in Figure1, it can be seen that atomic planes parallel to the planes of asymmetric GB and consisting of impurity Mg or Ni atoms alternate with planes filled with Al atoms, providing a complex pattern of the interacting atoms. Inside the band corresponding to the width of GB (atoms located inside the structural units in Figure 1), it is possible to distinguish several planes parallel to the boundary, differing in the interplanar spacing. The interplanar spacing are very unevenly distributed, and the filling of the nearest atomic planes with Al atoms and impurity atoms is also uneven. In [24], the number of cross sections for various types of GB, the interplanar spacing between them, and the pattern of filling with matrix atoms and impurity atoms are analyzed in detail. To understand their mutual arrangement, the distribution functions of $F(X)$ atoms of two grades along the width of grain boundaries were plotted in [24]. For each alloy and each of the asymmetric grain boundaries, atoms were isolated within the boundary width (X direction) on a single translation along Y and Z directions in the boundaries plane. For the isolated atoms, the fraction of atoms of this grade was calculated, located in the range $dX = 0.1$ Å, depending on the coordinate X along the direction perpendicular to the GB plane across its width. Figure 4 shows $F(X)$ functions for the simplest asymmetric GB for Al−Mg alloy. The values of the function and the point are plotted in blue and red for the matrix atoms and impurities in the alloys. In the same figures, the data for Al, obtained in a similar way, is shown in black for comparison. Each column for

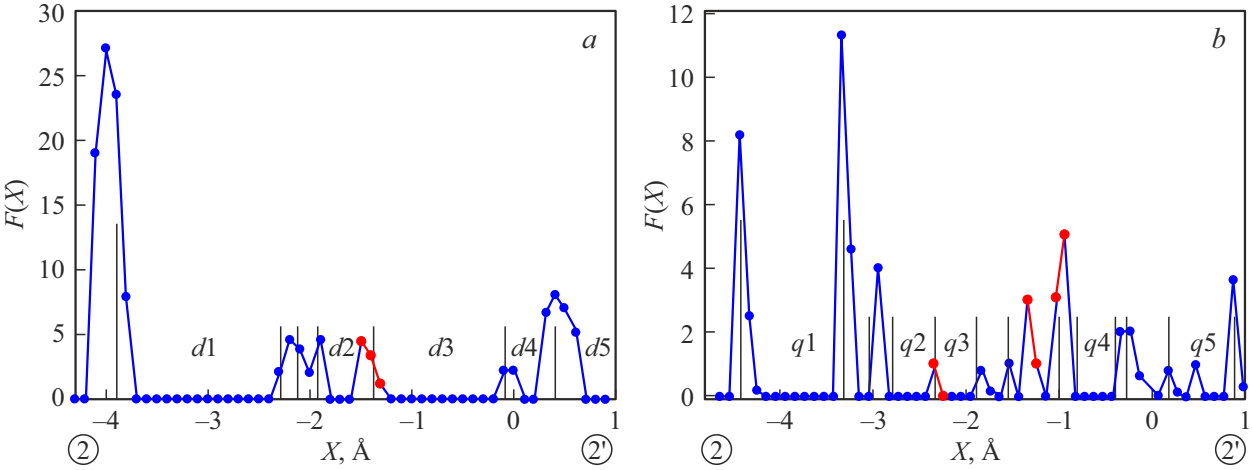

Figure 4. Function of atoms distribution across GB width $\Sigma5\{010\}/\{340\}\langle001\rangle$ (*a*) and GB $\Sigma5\{110\}/\{710\}\langle001\rangle$ (*b*) for Al and Al−Mg alloy [24]. Black vertical lines correspond to Al, blue and red dots — to Al−Mg alloy.

black Al atoms, separated from the other column by a gap, represents an atomic plane parallel to the boundary plane. In the left part of the figures the planes $\{001\}$ and $\{110\}$ are shown. They are more closely packed (higher columns), and the interplanar spacing ($d1$, $q1$ in Figure 4, *a, b*) is larger. On the right, the height of the columns decreases, and the interplane spacing ($d5$, $q5$ and $d3$, $q3$) also becomes shorter, which corresponds to a less closely packed planes $\{340\}$ and $\{710\}$. From the comparison of points for pure Al and Al−Mg alloy in the graph, it can be seen that the presence of impurity atoms in the boundary results in„blurring“ of each of the planes, which leads to both a change in interplanar spacing and, in some cases, to merging of planes. For GB $\Sigma5\{010\}/\{340\}\langle001\rangle$ (Figure 4, *a*) for the most closely-packed planes (sections) we may find a correlation between the sections for Al and Al−Mg. The distance between two closely spaced Mg layers is small, ~ 0.09 Å. For Al $\Sigma5\{110\}/\{710\}\langle001\rangle$ (Figure 4, *b*) the difference between the sections in Al and Al−Mg is larger and remains only near the extreme points across the GB width. Three layers of Mg atoms (red points in Figure 4, *b*) are standing relatively far from each other. The distance between the atomic layers makes ~ 0.53 Å and ~ 0.26 Å when moving from the left to the right in Figure 4, *b*. Even more complex situation is observed for Al−Ni alloy. Ni atoms have even a stronger effect (compared to Mg atoms) on the interplanar spacing inside GB and on merging some of the planes [24].

For all the above-mentioned sections of both asymmetric boundaries, the change in separation energy E^i_{sep} was calculated, similar to those shown in Figures 2, 3, for symmetric GB. However, the shape of $E^i_{\text{sep}}(X_i)$ curves is close to the curves in Figures 2, 3 only for several sections with a sufficiently large interplane spacing (e.g., sections $d1$ and $d3$ in Figure 4, *a*). The rest of $E^i_{\text{sep}}(X_i)$ curves have a complex, often not monotonous character of change. This is due, firstly, to the fact that Figure 1 shows superlattices with fully ordered regular filling of positions with Al atoms and impurity atoms in two layers parallel to the tilt axis $\langle001\rangle$. For other sections along the tilt axis, the filling is not as regular, which is due to the method of obtaining this superlattice (MD/MC at $T = 450$ K). Secondly, because of the above-mentioned uneven, often intersecting arrangement of various atomic planes parallel to the GB plane, a complex pattern of changes occurs in the interatomic interaction depending on the varied interplanar spacing X_i during separation.

In this study we calculated only the dependence of the decohesis energy $E_{\text{frac}}(N)$ on the cross-section number, calculated from the left to the right edge along the width of each of the asymmetric GB, and for each type of impurity atoms (Figure 5). The leftmost and rightmost points correspond to transcrystalline fracture in the matrix along the corresponding planes. From Figure 5 we see that in Al the fracture in all types of GB stands for the embrittlement.

Another situation is observed for Al−Mg alloy. The curves $E_{\text{frac}}(N)$ in Figure 5, *a, b* are inter-twined, the values of decohesis for Al and Al−Mg are located either higher or lower and close to each other. If Mg atoms are located in the closest position to this section (cross section *4* in Figure 5, *a* and cross section *5* in Figure 5, *b*), the decohesis energy for the alloy is higher than for pure Al. However, this excess of energy is small and makes (7−8) %. For the lowest values of E_{frac} for Al−Mg alloy, where fracture along GB could be expected (section *7* in Figure 5, *a* section *2* in Figure 5, *b*) the difference between the decohesis values is even smaller ~ 5 %. For calculations within MD framework, such a difference can generally be considered insignificant. The table shows an equally small contribution to strengthening or loss of strength in Al−Mg alloy and for symmetric GB in calculations, both within MD and *ab initio*.

The segregation of Ni on the asymmetric GB of the considered types significantly enhances the decohesis en-

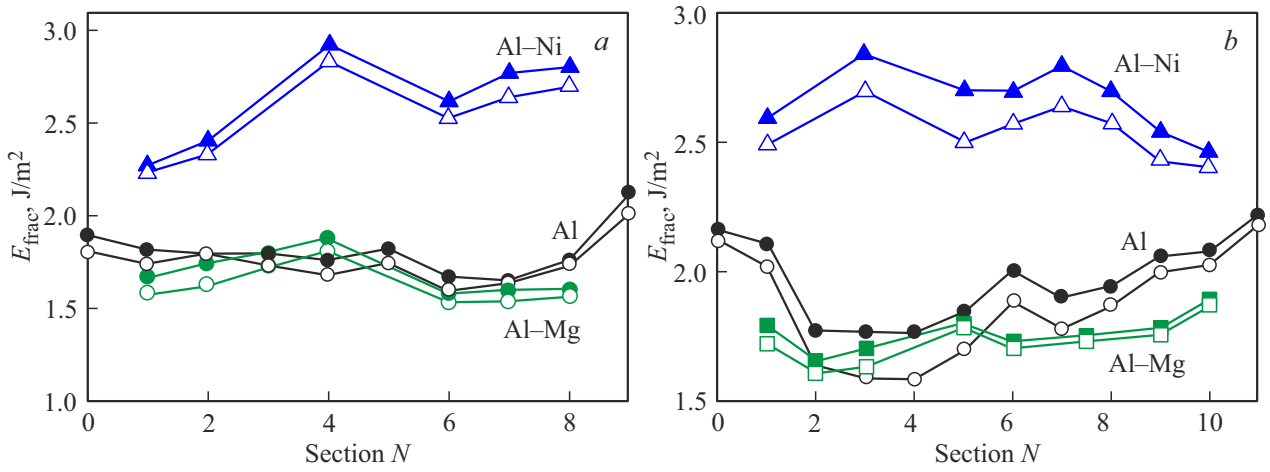

Figure 5. Decohesis energy versus the number of the cross-section for GB $\Sigma5\{010\}/\{340\}\langle001\rangle$ (*a*) and for GB $\Sigma5\{110\}/\{710\}\langle001\rangle$ (*b*). Black points correspond to Al, blue triangles — to Al–Ni alloy, green points — to Al–Mg alloy. Shaded symbols — without relaxation, non-shaded symbols — with relaxation.

ergy. Local peaks on the decohesis energy versus cross-section number curves for the asymmetric GB correspond to the planes located in the immediate vicinity of impurity atoms. In the points of maximum the values E_{frac} grow by $\sim (1.7-1.8)$ times. Thus, it can be argued that segregation of Ni atoms on GB of any type increases their strength.

4. Discussion of findings

In order to clarify the fracture specifics along the grain boundaries, atomistic modeling of crack opening was carried out within the rigid-grain-shift [15] in Al bicrystals and Al–3 at.%Mg and Al–3 at.%Ni alloys for symmetric and asymmetric grain boundaries containing ordered grain boundary segregations. By comparing the data from the table and in Figures 2, 3, 5 we may see that for all studied types of GB the decohesis energy E_{frac} is on average higher by ~ 1.5 times for Al–Ni alloy, compared to Al–Mg alloy. For the value σ_{max} this difference is even higher (excess in 1.7 times on average). However, for each of the alloys, the values E_{frac} and σ_{max} differ within $\sim 5\%$ depending on the GB type. Figure 5 clearly shows that the values of the decohesis energy in Al (black points) are close to the corresponding values of Al–Mg alloy, but significantly lower than for Al–Ni alloy. Thus, MD calculations show that Mg doping does not significantly change the strength properties of the considered symmetrical and asymmetric boundaries, whereas for Al–Ni alloy, the formation of grain boundary segregation on GB leads to a significant increase in their strength.

It is interesting to note that when comparing the results for Al and Al–Mg, Al–Ni alloys, it was found that the slippage resistance along GB for alloys increases significantly compared with Al [12,13]. This increase may be greater or less for one alloy or the other, depending on the direction of shear in the examined planes. Thus, when slipping along the tilt axis $\langle100\rangle$ for GB $\Sigma5\{013\}$ the values of energy for a non-stable grain-boundary stacking fault γ_{us} (maximal energy along the selected shift direction) grow in Al–Mg alloy compared to Al by ~ 2 times, for GB $\Sigma5\{012\}$ — by ~ 3.5 times. In Al–Ni alloy — for both GB γ_{us} rises by ~ 3 times. Thus, the effect of Mg and Ni in Al alloys on the characteristics of slippage and fracture along grain boundaries is ambiguous.

In [11], based on MD/MC and *ab initio* modeling, it was suggested that Mg and Ni may impact the microscopic mechanisms influencing the GB reconstruction specifics during the formation of ordered grain boundary segregations, which in turn affects the properties of slippage and decohesis in these Al alloys. The factors that significantly determine the development of the faceting process are the singularities of the chemical bond between the alloying element and the atoms of the matrix. By calculating the radial distribution function of Al atoms near the atom of the alloying element, it was shown that Mg segregation leads to a significant increase in the distance of Mg–Al to the nearest neighbors; this is especially pronounced in case of a dedicated asymmetric GB $\Sigma5\{010\}/\{340\}\langle001\rangle$. The ionic radius of both Mg and Ni exceeds the ionic radius of Al, but only in case of Mg is the deformation contribution to the atoms-matrix and GB interaction is prevailing [14]. In Al–Mg alloy, in which the interaction of Mg atoms with GB is controlled by a deformation mechanism, it is energetically advantageous for Mg atoms to be located in positions near the centers of structural units, where the greatest deformations and local expansion of the lattice are observed. This was illustrated in [14] also by calculating the distribution of local deformations determined by changing the bond lengths in the lattice. It is assumed that the presence of directional bonds, as in Al–Ni alloy, significantly alters the structure and properties

of GB. However, for Al−Ni an additional *ab initio* study is required.

Experimentally, it is believed that micro-doping of Mg, Zn, and Cu [4] in aluminum alloys significantly improves their properties. Using scanning electron microscopy and atom probe tomography, [25–27] it was found that these impurities form secretions near GB, therefore it is believed that they contribute to plasticity and increase the strength of GB. Another important proven fact is the significant effect of the above-mentioned impurities on the formation and stability of ultra-fine grains decorated with impurity atoms. It is this event that essentially shapes the unique properties of Mg, Zn and Cu aluminum alloys. In real NS polycrystals, the deformation behavior is more complex than that considered in atomistic modeling. A more realistic model should consider the presence of different types of grain boundaries, as well as the appearance of a spectrum of accommodative processes. Various scenarios of deformation of nanostructured materials were considered, mainly related to the processes occurring at GB: grain boundary slippage and nucleation of microcracks in the triple joints of grains caused by the transfer of deformation along the GB from one grain to another [16,17]. However, we believe that the results obtained in this work clearly demonstrate the correlation between the chemical bonding of impurity atoms, their segregation behavior, and the strength characteristics of the grain boundaries.

5. Conclusion

In order to clarify the fracture specifics along the grain boundaries, atomistic modeling of crack opening was carried out within the rigid-grain-shift in Al bicrystals and Al−3 at.%Mg and Al−3 at.%Ni alloys for the grain boundaries with the tilt axis ⟨001⟩containing ordered grain boundary segregations. The susceptibility to fracture along the symmetric GB Σ5, as well as along the asymmetric GB $\Sigma5\{010\}/\{340\}\langle001\rangle$ and $\Sigma5\{110\}/\{710\}\langle001\rangle$ in bicrystals of Al−Mg and Al−Ni alloys was studied based on the decohesis energy analysis. It has been found that the fracture resistance according to GB for Al−Ni alloy increases significantly compared with Al. For Al−Mg, the effect of Mg segregation on GB was weak, ambiguous, and depended on the type of plane within GB width along which the fracture occurred.

Funding

The study was conducted under the state assignment of the Ministry of Education and Science of the Russian Federation for the Institute of Metal Physics, Ural Branch of the Russian Academy of Sciences

Conflict of interest

The authors report no conflict of interest.

References

[1] P.Lejček. Grain boundary segregation in metals. Springer Series Mater. Sci., N.Y. (2010).
[2] Priester L. Grain Boundaries: From Theory to Engineering. Springer Series in Mater. Sci. N.Y. (2014).
[3] B.B. Straumal, O.A. Kogtenkova, A.S. Gornakova, V.G. Sursaeva, B. Baretzky. J. Mater. Sci. **51**, 382 (2016).
[4] G. Sha, L. Yao, X. Liao, S.P. Ringer, Z.C. Duan. Ultramicroscopy **111**, 500 (2011).
[5] X. Liu, X. Wang, J. Wang, H.J. Zhang. J. Phys.: Condens. Matter. **17**, 4301 (2005).
[6] S. Zhang, O.Y. Kontsevoi, A.J. Freeman, G.B. Olson. Acta Materialia **59**, 6155 (2011).
[7] R.G. Song, M.K. Tseng, B.J. Zhang, J. Liu, Z.H. Jin, K.S. Shin. Acta Mater. **44**, 3241 (1996).
[8] V.I. Razumovskiy, A.V. Ruban, I.M. Razumovskii, A.Y. Lozovoi, V.N. Butrimb, Y.K. Vekilov. Scr. Mater. **65**, 926 (2011).
[9] D. Zhao, O. M.Løvvik, K. Marthinsen, Y. Li. Applied Physics Letters **100**, 231904 (2012).
[10] L.E. Kar'kina, I.N. Kar'kin, A.R. Kuznetsov, Yu.N. Gornostyrev. FTT **60**, 1974 (2018) (in Russian).
[11] L. Karkina, I. Karkin, A. Kuznetsov, Y. Gornostyrev. Metals **9**, 1319 (2019).
[12] L.E. Kar'kina, I.N. Kar'kin, Yu.N. Gornostyrev. FMM **121**, 901 (2020) (in Russian).
[13] L.E. Kar'kina, I.N. Kar'kin, Yu.N. Gornostyrev. FMM **122**, 1187–1195 (2021 (in Russian).
[14] L.E. Kar'kina, I.N. Kar'kin, Yu.N. Gornostyrev. FMM **123**, 1079 (2022) (in Russian).
[15] S. Zhang, O.Y. Kontsevoi, A.J. Freeman, G.B. Olson. Acta Mater. **59**, 6155 (2011)
[16] I.A. Ovid'ko, R.Z. Valiev, Y.T. Zhu. Prog. Mater. Sci. **94**, 462 (2018)
[17] I.A. Ovid'ko, A.G. Sheinerman. Acta Mater. **52**, 1201–1209 (2004).
[18] M.A. Tschopp, D.L. Macdowell. Philos. Mag. **87**, 3871–3892 (2007).
[19] Y.-M. Kim, N.J. Kim, B.-J. Lee. Calphad **33**, 650 (2009).
[20] G.P. P.Pun, Y. Mishin. Philos. Mag. **89**, 3245 (2009).
[21] A. Kuznetsov, L. Karkina, Yu. Gornostyrev, P. Korzhavyi. Metals **11**, 631 (2021).
[22] S. Plimpton. J. Comput. Phys. **117**, *1*, 1 (1995).
[23] C. Hu, R. Dingreville, B.L. Boyce. Comput. Mater. Sci. **232**, 112596 (2024).
[24] L.E. Kar'kina, I.N. Kar'kin, Yu.N. Gornostyrev. FMM **126**, 943-949 (2025) (in Russian).
[25] X. Sauvage, G. Wilde, S.V. Divinski, Z. Horita, R.Z. Valiev. Mater. Sci. Eng. A **540**, 1-12 (2012).
[26] R.Z. Valiev. Nature **419**, 887 (2002).
[27] X. Sauvage, N. Enikeev, R. Valiev, Y. Nasedkina, M. Murashkin. Acta Mater. **72**, 125-136 (2014).

Translated by T.Zorina